ACS NANO
Cite This: *ACS Nano* 2020, 14, 1148−1157
www.acsnano.org

Enhanced Chemical Immobilization and Catalytic Conversion of Polysulfide Intermediates Using Metallic Mo Nanoclusters for High-Performance Li−S Batteries

Yuanjian Li,[†] Chong Wang,[†] Wenyu Wang,[†] Alex Yong Sheng Eng,[‡] Mintao Wan,[†] Lin Fu,[†] Eryang Mao,[†] Guocheng Li,[†] Jiang Tang,[†] Zhi Wei Seh,[‡] and Yongming Sun*,[†]

[†]Wuhan National Laboratory for Optoelectronics, Huazhong University of Science and Technology, Wuhan 430074, China
[‡]Institute of Materials Research and Engineering, Agency for Science, Technology and Research (A*STAR), 2 Fusionopolis Way, Innovis, Singapore 138634, Singapore

Supporting Information

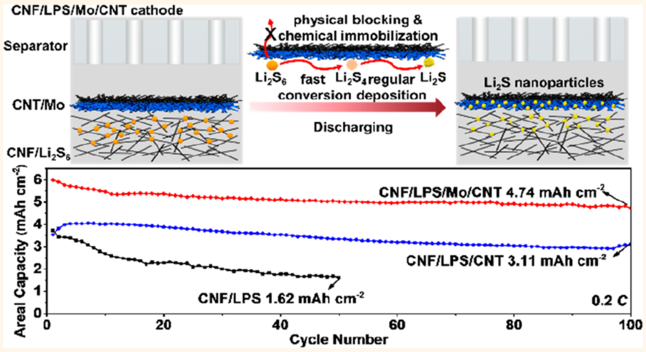

ABSTRACT: Rechargeable lithium−sulfur batteries have attracted tremendous scientific attention owing to their high energy density. However, their practical application is greatly hindered by the notorious shuttling of soluble lithium polysulfide (LPS) intermediates with sluggish redox reactions and uncontrolled precipitation behavior. Herein, we report a semiliquid cathode composed of an active LPS solution/carbon nanofiber (CNF) composite layer, capped with a carbon nanotube (CNT) thin film decorated with metallic Mo nanoclusters that regulate the electrochemical redox reactions of LPS. The trace amount (0.05 mg cm^{-2}) of metallic Mo on the CNT film provides sufficient capturing centers for the chemical immobilization of LPS. Together with physical blocking of LPS by the compact CNT film, free diffusion of LPS is significantly restrained and the self-discharge behavior of the Li−S cell is thus effectively suppressed. Importantly, the metallic Mo nanoclusters enable fast catalytic conversion of LPS and regular deposition of lithium sulfide. As a result, the engineered cathode exhibits a high active sulfur utilization (1401 mAh g^{-1} at 0.1 C), stable cycling (500 cycles at 1 C with 0.06% decay per cycle), high rate performance (694 mAh g^{-1} at 5 C), and low self-discharge rate (3% after 72 h of rest). Moreover, a high reversible areal capacity of 4.75 mAh cm^{-2} is maintained after 100 cycles at 0.2 C for a cathode with a high sulfur loading of 7.64 mg cm^{-2}. This work provides significant insight into the structural and materials design of an advanced sulfur-based cathode that effectively regulates the electrochemical reactions of sulfur species in high-energy Li−S batteries.

KEYWORDS: *lithium−sulfur batteries, semiliquid cathode, metallic Mo nanoclusters, chemical immobilization, catalytic conversion*

Rechargeable lithium−sulfur (Li−S) batteries feature high theoretical energy density (2567 W h kg^{-1}), low cost, and abundance of raw materials and have been regarded as one of the most promising next-generation energy storage systems for electric vehicles and grid-level storage.[1−3] Nevertheless, the applications of Li−S batteries are still subject to their low practical energy density, limited power density, and short cycle life.[4−6] The sulfur cathode suffers from high electronic/ionic resistivity of sulfur, the "shuttle effect" of lithium polysulfide (LPS) intermediates, and noticeable volume fluctuation of sulfur species during the charge/discharge processes, which together lead to rapid capacity fading, low Coulombic efficiency, and severe self-discharge.[7−9]

To address these issues, various nanostructured sulfur/carbon (S/C) electrodes have been fabricated through a conventional slurry casting process and considerable achievement in electrochemical performance has been realized, including high specific capacity (>1300 mA h g^{-1}) and long cycle life (<0.1% capacity fading per cycle) at low active mass loading of sulfur (e.g., <2 mg cm^{-2}).[10−12] However, electrode films on flat aluminum foil fabricated using a slurry casting method usually

Received: November 18, 2019
Accepted: December 13, 2019
Published: December 13, 2019

DOI: 10.1021/acsnano.9b09135

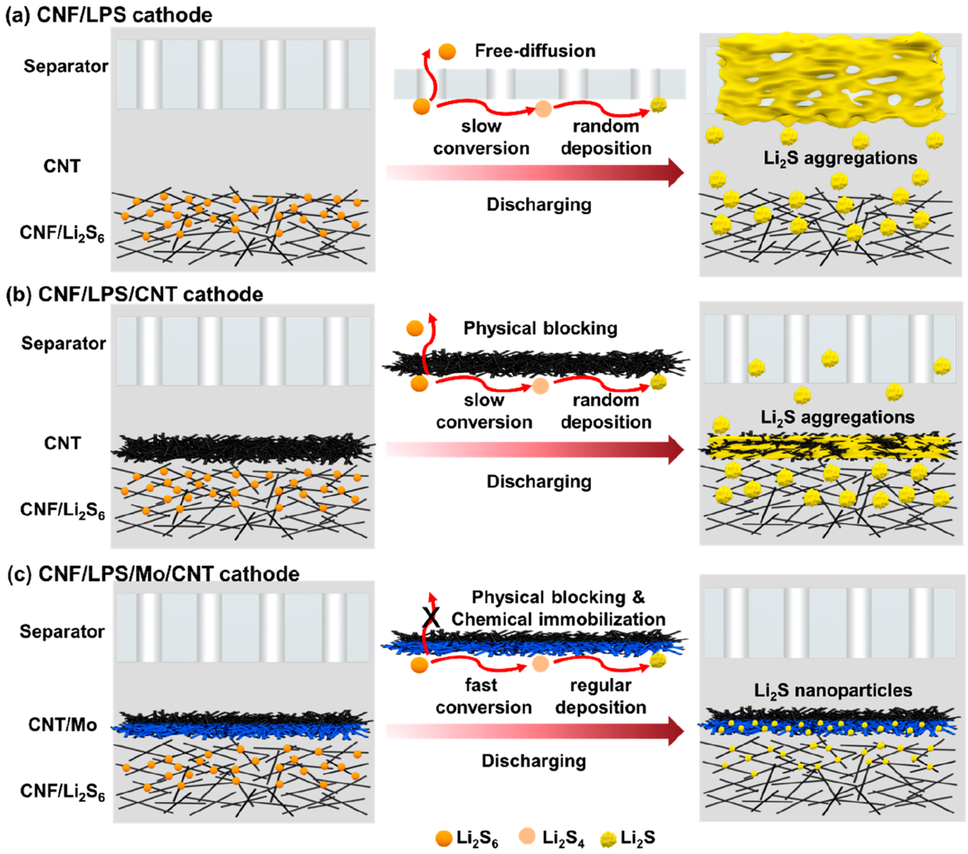

Figure 1. Schematic illustration of the electrochemical behavior of the LPS catholyte with different electrode configurations: (a) CNF/LPS, (b) CNF/LPS/CNT, and (c) CNF/LPS/Mo/CNT cathodes. The designed CNF/LPS/Mo/CNT cathode could effectively address the free diffusion of LPS, catalyze their fast conversion, and realize regular deposition of lithium sulfide (Li_2S) nanoparticles during discharge.

exhibit slow ionic/electronic migration at an industrial-level areal capacity (~3.5 mAh cm^{-2}, corresponding to ~4 mg cm^{-2} of sulfur loading). Due to repeated volume expansion/contraction cycles, they also pulverize easily or detach off from the current collector, leading to low sulfur utilization and inferior cycling stability.

Recently, "semi-liquid cathodes" have been widely investigated, which consists of a liquid LPS catholyte and a solid free-standing carbon structure, such as graphene, carbon nanotube, or carbon nanofiber.[13−15] The semiliquid electrode configuration enables uniform distribution of active materials throughout the conductive matrix, which not only facilitates kinetics of the Li−S redox reactions and increases the utilization of active materials but also prevents pulverization of the entire electrode caused by the volume change during cycling.[16−18] Compared with the traditional sulfur-based electrodes achieved by a slurry casting method, the semiliquid sulfur-based cathodes often show higher specific capacities and gravimetric energy densities of Li−S batteries at high active mass loading (e.g., >4 mg cm^{-2}).[19−21] However, they still suffer from inadequate capacity retention and rate capability, due to the weak confinement effect of polar polysulfide anions in nonpolar carbon materials and the inferior contact between them (Figure 1a).

To circumvent the above issues, various metals and metal compounds have been incorporated into carbonaceous materials to construct composite polysulfide reservoirs (e.g., Pt/graphene, TiO_2/graphene, TiN/N-doped graphene, SnS_2/graphene, and MXene/reduced graphene oxide) due to their strong chemical immobilization and catalytic conversion of polysulfides.[22−31] Despite this exciting progress, several challenges still plague the further development and practical applications of the semiliquid sulfur-based cathode: (1) The large proportion (>15 wt %) of electrochemical inert inorganic materials in the as-prepared cathodes considerably reduces the overall capacity of the cathodes.[22−28] (2) These inorganic materials exhibit inferior electrical conductivity and large particle size, which might greatly impede the electron migration and lower the number of accessible active sites.[32−34] (3) Limited attention has been paid to the regulation of the deposition of insulating lithium sulfide on these composite matrixes, which plays an important role in achieving high sulfur utilization.[35−39] The random deposition of lithium sulfide aggregates on the carbon current collector results in electrode passivation and consequent large polarization of the electrode, hindering the realization of high-rate Li−S batteries (Figure 1b).

Herein, we fabricate a semiliquid cathode composed of an active lithium polysulfide (Li_2S_6, LPS) solution/carbon nanofiber (CNF) composite layer capped with a carbon nanotube (CNT) thin film, decorated with metallic Mo nanoclusters that regulate the electrochemical reactions of sulfur species. The large interspace of the interwoven CNF substrate allows the uniform dispersion of active LPS solution. Its porous structure accommodates the volume changes during cycling, and its interconnected network affords continuous electronic contacts between the CNF and LPS. The interwoven CNF network, together with the compact and dense

DOI: 10.1021/acsnano.9b09135
ACS Nano 2020, 14, 1148−1157

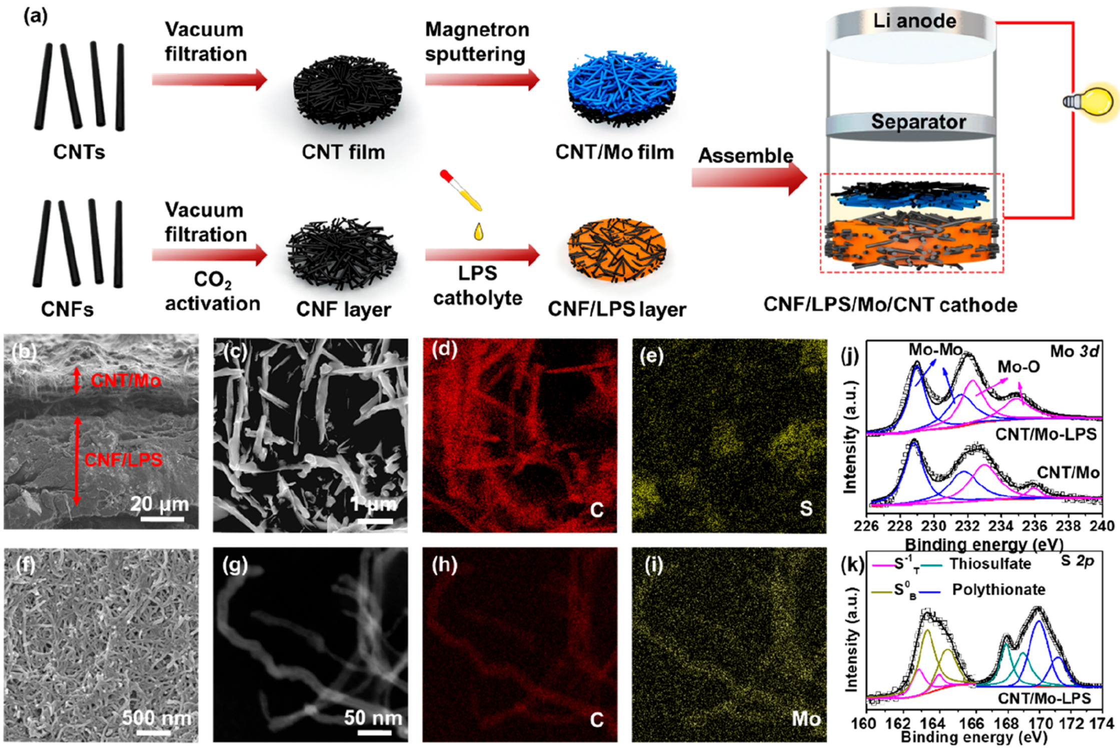

Figure 2. (a) Fabrication of the CNF/LPS/Mo/CNT cathode. (b) Cross-section SEM images of the CNF/LPS/Mo/CNT cathode showing the CNT/Mo cap layer and the CNF/LPS layer. (c) Top-view SEM images of the CNF/LPS layer of the CNF/LPS/Mo/CNT electrode and the corresponding mapping of (d) C and (e) S elements. (f) Top-view SEM images of the CNT/Mo cap layer of the CNF/LPS/Mo/CNT electrode. (g) TEM images of CNT/Mo composites and the corresponding mapping of (h) C and (i) Mo elements. (j) Mo 3d XPS spectra of the CNT/Mo composites without and with LPS. (k) S 2p spectrum of CNT/Mo composites with LPS.

CNT cap upper layer, physically confines the active LPS at the cathode side. Meanwhile, the metallic Mo nanoclusters on the CNT film not only offer numerous chemical binding sites to trap the soluble LPS but also propel the redox conversion from long-chain LPS to short-chain LPS, and then to Li_2S. Due to the improved immobilization and redox conversion of LPS, the deposition of lithium sulfides is regulated and the accumulation of large agglomerates on the surface of the bottom CNF substrate is avoided (Figure 1c). It is worthwhile to note that only a small amount of metallic Mo nanoclusters is required (0.05 mg cm^{-2}) in the composite electrode, which helps to retain a high overall capacity of sulfur-based cathodes. Due to the advantageous design of cathode structure and composition, the as achieved cathode shows good electrochemical properties including a stable cycling stability (0.06% capacity decay per cycle for 500 cycles at 1 C), a superior rate capability (694 mAh g^{-1} at 5 C), as well as a low self-discharge rate. Even at a high sulfur loading of 7.64 mg cm^{-2}, the electrode exhibits a high reversible areal capacity of 4.75 mAh cm^{-2} after 100 cycles at 0.2 C.

RESULTS AND DISCUSSION

The fabrication of the CNF/LPS/Mo/CNT cathode is illustrated in Figure 2a. To prepare the cap layer (CNT/Mo nanocomposite film) of the CNF/LPS/Mo/CNT electrode, a CNT film was first achieved through a simple vacuum filtration method using a commercial polypropylene (PP) separator as the filter membrane and then ultrafine metallic Mo nanoclusters were deposited on the surface of the CNT layer through a magnetron sputtering process. Meanwhile, a free-standing CNF framework was prepared through vacuum filtration followed by an activation process in the CO_2 atmosphere.[14,39] A CNF/LPS composite layer was achieved after the injection of the Li_2S_6 catholyte into the porous CNF film. After overlapping the two layers, a CNF/LPS/Mo/CNT composite cathode was formed. The CNT-based layer has a dense network structure to block the diffusion of LPS due to the small diameter (~15 nm) of CNTs, while the CNF layer has a large void space due to the much larger diameter (~150 nm) of CNFs, which is beneficial for the trapping of LPS. Figure 2b shows the cross-section SEM images of a typical CNF/LPS/Mo/CNT cathode. The electrode consists of a CNT/Mo cap layer and a CNF/LPS layer with a thickness of ~5 and 50 μm, respectively. The SEM image of the CNF/LPS composite exhibits a cross-linked 3D CNF network with large interspaces (0.2−2 μm) (Figure 2c). The results of energy-dispersive X-ray (EDX) elemental mapping indicate the uniform distribution of active sulfur species within the interspace of the CNF network (Figure 2d and e). The top-view SEM image of the CNT film displays its interconnected and compact architecture (Figure S3). After decorating with the Mo metal, there is no obvious change in morphology, and the compact structure of the CNT/Mo films is beneficial for forming a physical barrier to block polysulfide migration (Figure 2f). The CNT and CNT/Mo cap layers improve the electrolyte wettability (Figure S4), which is expected to facilitate Li-ion diffusion through the separator and propel the conversion of LPS. The scanning transmission electron microscopy (STEM) image and corresponding EDX elemental mappings of C and Mo of the CNT/Mo nanocomposites in Figure 2g−i also reflect the uniform distribution of metallic Mo nanoclusters on the surface of CNTs. X-ray diffraction (XRD)

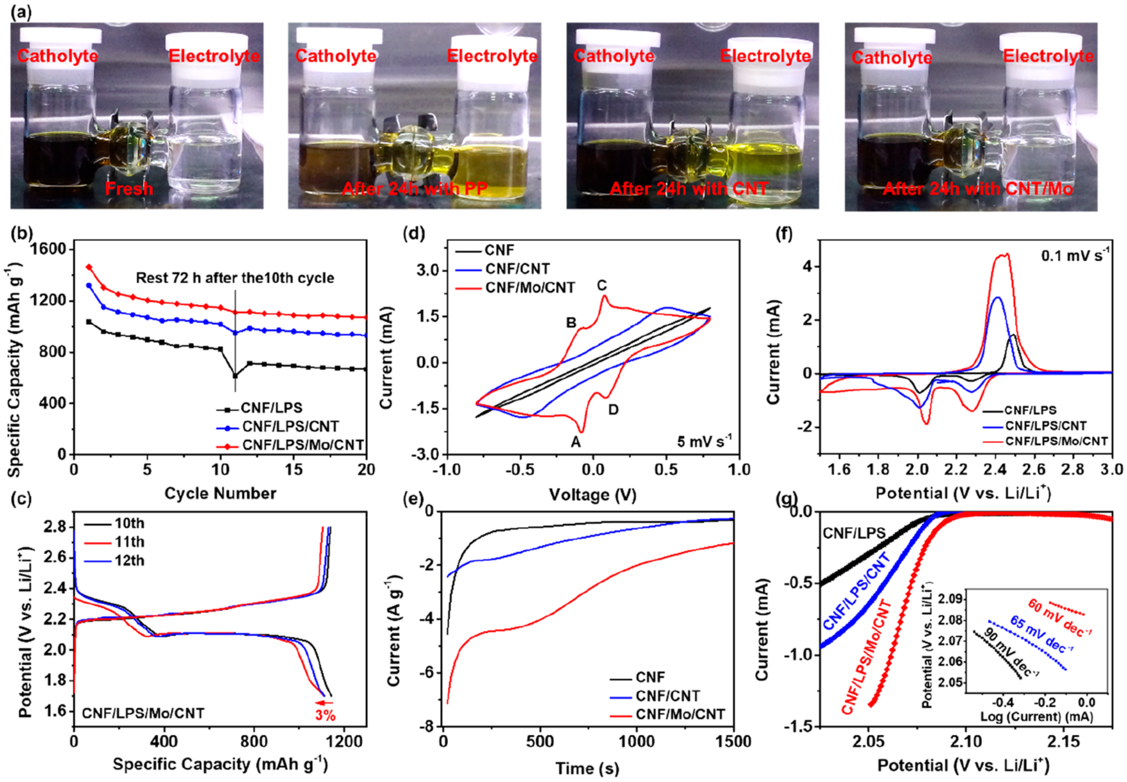

Figure 3. (a) Optical images for the polysulfide diffusion test in glass cells with pure PP separator and PP separator with CNT and CNT/Mo films, respectively. (b) Self-discharge rate tests of the CNF/LPS, CNF/LPS/CNT, and CNF/LPS/Mo/CNT cathodes with a resting time of 72 h at a full charge state after the 10th cycle at 0.1 C. (c) Representative charge−discharge voltage profiles for the 10th, 11th, and 12th cycles and average self-discharge rate of cells with a CNF/LPS/Mo/CNT cathode. (d) CV curve of symmetric cells employing CNF/Mo/CNT, CNF/CNT, and CNF electrodes at a scan rate of 5 mV s^{-1}. (e) Current−time curves from the potentiostatic discharging from the open-circuit condition (2.2 V) to 2 V. (f) CV profiles of the CNF/LPS, CNF/LPS/CNT, and CNF/LPS/Mo/CNT cathodes at a scan rate of 0.1 mV s^{-1}. (g) Potentiostatic polarization curves of CNF/LPS, CNF/LPS/CNT, and CNF/LPS/Mo/CNT cathodes at a scan rate of 0.1 mV s^{-1} for their reduction processes. The inset shows the corresponding Tafel plots derived from the potentiostatic polarization curves.

patterns further indicate a body-center cubic structure of Mo nanocrystal on the CNT film (Figure S5).[34] Notably, the mass loading of the metallic Mo layer is as low as 0.05 mg cm^{-2} (5 wt % of the entire polysulfide reservoir), much lower than the typical values of 15−50 wt % for metal compounds in sulfur-based cathodes (Table S1). The low mass loading of the electrochemically inert material helps to achieve a practical high energy density of Li−S batteries.

The surface electronic state of elemental Mo was investigated by X-ray photoelectron spectroscopy (XPS). As shown in Figure 2h, the Mo 3d spectrum can be deconvoluted into four peaks. The first two peaks located at 228.8 and 231.9 eV are assigned to the Mo−Mo bond for metallic Mo (Mo^0).[34,40] The other two peaks at 233.0 and 236.1 eV suggest the presence of MoO_x species, which probably results from the oxidation of metallic Mo in air.[41] After loading with LPS solution in the CNT/Mo composite, negative shifts for the peaks of MoO_x species are observed in the high-resolution XPS Mo 3d spectra (Figure 2j), which suggests the electrons transfer from the electronegative S atoms of LPS species to the electropositive Mo atoms of MoO_x species. The appearance of thiosulfate and polythionate signals in the high-resolution S 2p spectrum (Figure 2k) further confirms the ability of oxidized molybdenum species in chemically oxidizing polysulfide ions into thiosulfate and polythionate species.[42,43] Such chemical interactions between the MoO_x species and LPS also receive strong evidence from the Raman analyses (Figure S6) and have high chemisorption energy for polysulfides (4.07−7.51 eV).[44,45] Additionally, the metallic Mo (Mo^0) peaks in the Mo 3d spectrum of the CNT/Mo-LPS composites exhibit a shift to higher binding energy in comparison with that of the pristine Mo 3d spectrum, which illustrates the interaction between the polysulfides and metallic Mo. The sulfur-passivated Mo metal surface possesses efficient binding sites for LPS with a binding energy between 0.5 and 2.5 eV.[34,46] The chemical immobilization of LPS on these Mo metallic nanoclusters, together with the physical blocking effect of the CNT/Mo layer, can suppress the diffusion of soluble LPS. Thus, enhanced capacity retention and Coulombic efficiency of the CNF/LPS/Mo/CNT cathode can be expected.

A visualized setup was used to investigate the role of the functional CNT/Mo layer in blocking the transportation of LPS (Figure 3a and Figure S7). Glass cells were assembled with the right chamber containing bare ether-based electrolyte and the left chamber containing LPS in the same electrolyte using a pristine PP separator, a PP separator with CNT, and a PP separator with CNT/Mo, respectively.[47,48] In the cell using the pristine separator, the bare electrolyte in the right chamber turned light yellow after only 5 min and became brown after 24 h, which suggests the easy diffusion of LPS through the regular separator. In contrast, the migration of LPS across the separator with CNT is retarded. Only a slight color change is observed for the electrolyte in the right chamber after 24 h, benefiting from physical interception by the dense CNT layer.

DOI: 10.1021/acsnano.9b09135
ACS Nano 2020, 14, 1148−1157

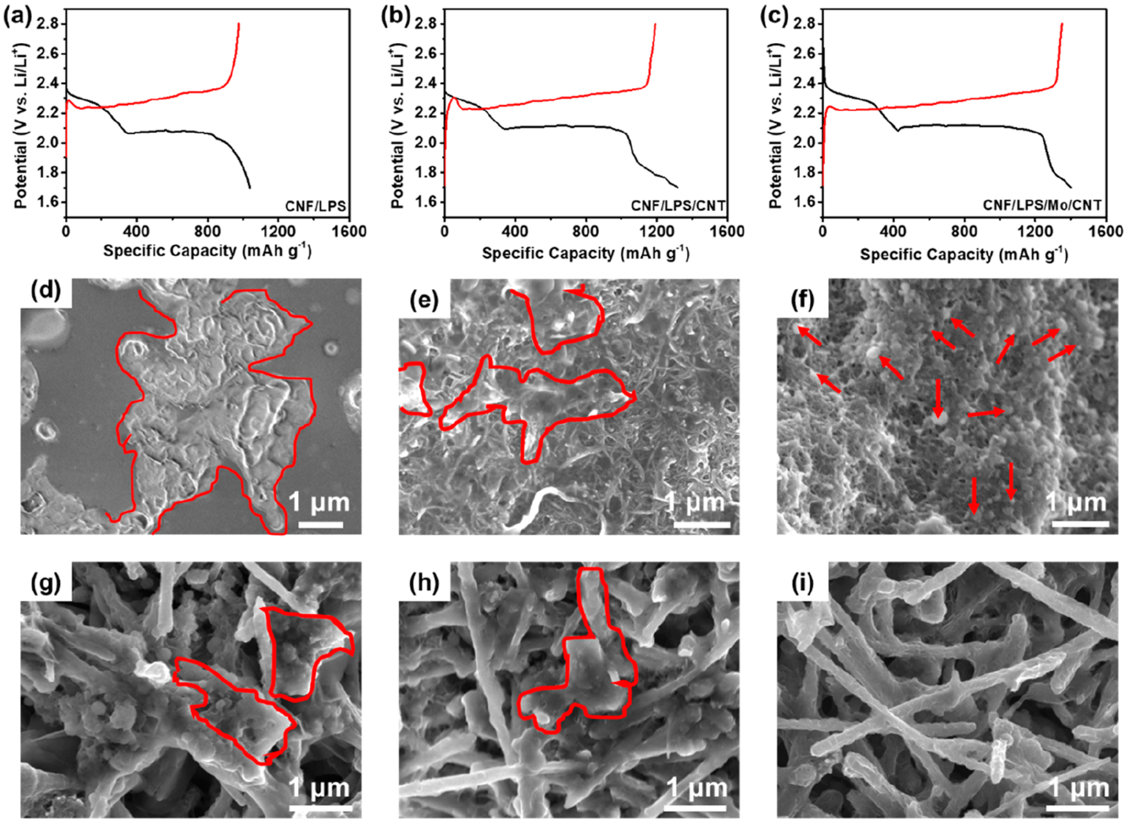

Figure 4. First-cycle charge and discharge curves of the (a) CNF/LPS, (b) CNF/LPS/CNT, and (c) CNF/LPS/Mo/CNT cathodes at 0.1 *C*. SEM images of (d) the PP separator for the cell with the CNF/LPS cathode, (e) the CNT layer of the CNF/LPS/CNT cathode, and (f) the CNT/Mo layer of the CNF/LPS/Mo/CNT cathode after the first discharge process. SEM images of the CNF layer of the (g) CNF/LPS, (h) CNF/LPS/CNT, and (i) CNF/LPS/Mo/CNT cathode after the first discharge process.

When the separator with CNT/Mo is employed, nearly no color change is observed for the electrolyte in the left chamber after 24 h. Therefore, this conspicuous improvement in inhibiting Li_2S_6 diffusion using the CNT/Mo separator comes from both the chemical immobilization by metallic Mo nanoclusters and physical blocking by the compact CNT/Mo network, as discussed in Figure 2h and i.

The self-discharge behavior of Li−S cells using different cathodes was investigated under a current rate of 0.1 *C*. Typically, Li−S coin cells were fabricated using lithium metal as the anode and CNF/LPS, CNF/LPS/CNT, or CNF/LPS/Mo/CNT electrode as the cathode, respectively. The sulfur mass loading for the cathodes was 1.92 mg cm^{-2} (10 μL of 0.5 M Li_2S_6 catholyte). The cells were continuously charged and discharged for 10 cycles, then rested for 72 h after they were fully charged to 2.8 V, and finally further cycled for 20 cycles.[49,50] During the interrupted rest period, the voltage of the cells with the CNF/LPS cathode and CNF/LPS/CNT cathode exhibited a fast decline to 2.23 and 2.32 V, respectively, while the cell with a CNF/LPS/Mo/CNT cathode sustained a more stable voltage during the rest, suggesting that the self-discharge of the cell is reduced (Figure S8). For more clarity, the self-discharge rate was calculated on the basis of the ratio of the lost discharge capacity to the initial capacity $[(Q_{10th} - Q_{11th})/Q_{10th}]$. A significant loss of discharge capacity is observed for the 11th cycle of the CNF/LPS cathode, corresponding to a high self-discharge rate of 17% (Figures 3b and S9). The capacity loss is decreased for the cell with a CNF/LPS/CNT cathode due to physical blocking of the LPS by the CNT layer. Notably, the cell using the CNF/LPS/Mo/CNT cathode affords a weak self-discharge rate of 3% after its storage at the fully charged state for 72 h (Figure 3c), indicating that the self-discharge behavior is effectively retarded. The suppressed self-discharge behavior of the CNF/LPS/Mo/CNT cathode originates from the incorporation of CNT/Mo that acts as an efficient physical shield and chemical anchor of polysulfides.

To identify the effectiveness of the metallic Mo nanoclusters on the electrocatalysis of LPS intermediates, symmetric cells using CNF/Mo/CNT as the identical working and counter electrode were assembled with 0.5 M Li_2S_6 electrolyte. Its cyclic voltammetry (CV) profile in a voltage window from −0.7 to 0.7 V at a scan rate of 5 mV s^{-1} (Figure 3d) displays four distinct peaks at −0.081 V (peak A), −0.090 V (peak B), 0.076 V (peak C), and 0.092 V (peak D), which can be assigned to the electrochemical reactions of Li_2S_6. Specifically, peak A is due to the reduction of Li_2S_6 to Li_2S, peak B is accompanied by the oxidation of Li_2S to reconstitute Li_2S_6, peak C is associated with the generation of elemental S_8 by the further oxidation of Li_2S_6, and peak D arises from the reduction of S_8 to Li_2S_6.[51] In comparison, there are no peaks observed for the CNF/CNT and CNF counterparts in their CV profiles (Figure 3d). Thus, the metallic Mo affords outstanding electrocatalytic activity for propelling polysulfide conversion. Furthermore, the Nyquist plots (Figure S10) show charge transfer impedance of 8.1, 28.6, and 36.9 Ω for the CNF/Mo/CNT, CNF/CNT, and CNF symmetric cells, respectively. These results suggest the good electrical

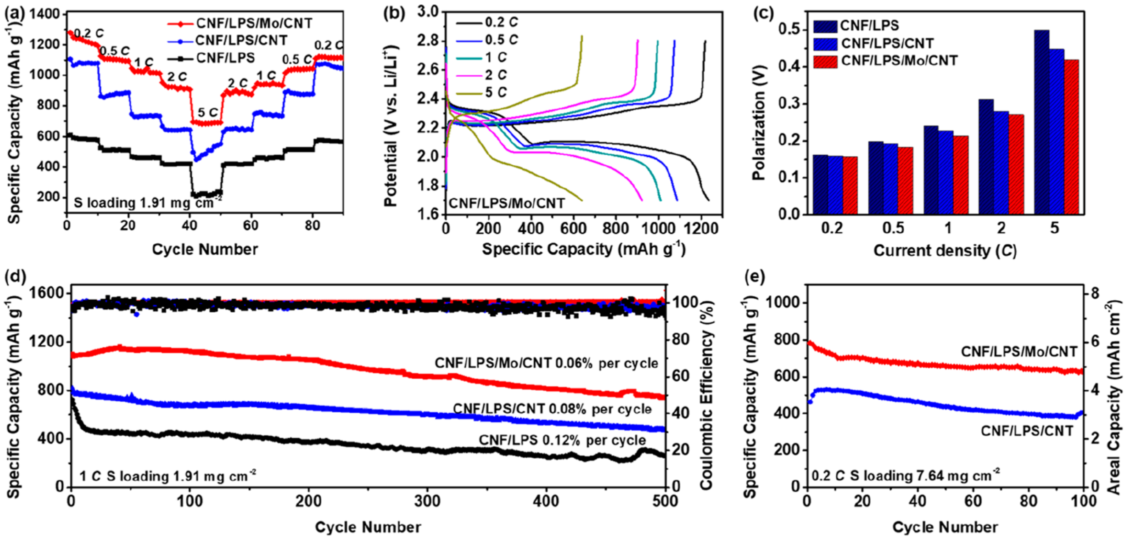

Figure 5. (a) Rate capability of the CNF/LPS, CNF/LPS/CNT, and CNF/LPS/Mo/CNT cathodes. (b) Charge−discharge profiles of the CNF/LPS/Mo/CNT cathode at different current densities. (c) Polarization potentials of the CNF/LPS, CNF/LPS/CNT, and CNF/LPS/Mo/CNT cathodes at different current densities. (d) Long-term cycling performance of the CNF/LPS, CNF/LPS/CNT, and CNF/LPS/Mo/CNT cathodes at 1 C. (e) Cycling performance of the CNF/LPS/Mo/CNT cathode with high sulfur mass loading of 7.64 mg cm^{-2} at 0.2 C.

conductivity of CNF/Mo/CNT and favorable charge transfer kinetics at the CNF/Mo/CNT interface.[51,52] The current−time response from the potentiostatic discharge measurement is usually used to verify the effectiveness of the catalyst to promote the Li_2S precipitation.[52,53] As shown in Figure 3e, the CNF/Mo/CNT electrode presents the highest precipitation current among the three tested samples (CNF, CNF/CNT, CNF/Mo/CNT), indicating the improvement of the Li_2S precipitation kinetics for the electrode with the decoration of Mo nanoclusters.[52,53] The above results confirm the catalytic effect of the metallic Mo in polysulfide conversion and Li_2S precipitation.

We further investigated the fast sulfur transformation chemistry on the CNF/LPS/Mo/CNT cathode in actual Li−S coin cells through CV measurement. From the CV profiles in Figure 3f, two cathodic peaks located at 2.28 and 2.05 V could be observed, which are attributed to the electrochemical transformation from soluble long-chain LPS to short-chain LPS and the subsequent insoluble Li_2S. In the oxidation process, there exists a significant anodic peak at 2.40 V, which is known to be the reversible conversion of Li_2S to LPS and finally to elemental sulfur.[23,54] A distinguishable positive shift in the cathodic peak and a negative shift in the anodic peak are observed for the CNF/LPS/Mo/CNT cathode along with a much higher current density compared to that of the CNF/LPS and CNF/LPS/CNT cathodes, revealing the improved reaction kinetics of the CNF/LPS/Mo/CNT cathode due to the catalytic effect of the metallic Mo nanoclusters. Recent studies demonstrated that the liquid−solid reactions from short-chain LPS to Li_2S have a significant influence on the sulfur utilization.[31,55] Here potentiostatic polarization experiments were carried out to further investigate the effect of metallic Mo nanoclusters on the charge-transfer kinetics during the short-chain LPS lithiation process.[56,57] Polarization curves demonstrate that the CNF/LPS/Mo/CNT cathode possesses an onset potential of 2.11 V, which was higher than 2.07 V for the CNF/LPS cathode and 2.08 V for the CNF/LPS/CNT cathode (Figures 3g and S12). Furthermore, the CNF/LPS/Mo/CNT cathode presents a Tafel slope of 60 mV dec^{-1} and an exchange current density of 75 μA cm^{-2}. In contrast, the CNF/LPS electrode has a Tafel slope of 90 mV dec^{-1} and an exchange current density of 24 μA cm^{-2} and the CNF/LPS/CNT cathode shows a Tafel slope of 65 mV dec^{-1} and an exchange current density of 35 μA cm^{-2}. These results again suggest the improved liquid−solid reactions for the CNF/LPS/Mo/CNT cathode with the assistance of metallic Mo nanoclusters (Figure S12).

Figure 4a−c compares the first-cycle galvanostatic discharge/charge voltage profiles of the CNF/LPS, CNF/LPS/CNT, and CNF/LPS/Mo/CNT cathodes at 0.1 *C* (1 *C* = 1675 mA g^{-1}), respectively. All of the electrodes display two characteristic discharge plateaus of sulfur cathodes. The CNF/LPS/Mo/CNT electrode has a higher discharge capacity (1401 mAh g^{-1}) with higher active material utilization (84%) than the CNF/LPS (1037 mAh g^{-1}, 62%) and CNF/LPS/CNT (1320 mAh g^{-1}, 79%) cathodes, suggesting effective LPS immobilization and enhanced reaction kinetics. After the first discharge process, abundant solid lithium sulfide (Li_2S/Li_2S_2) aggregates with a size of several micrometers emerge on the surfaces of the PP separator for the Li−S cell with the CNF/LPS cathode and the CNT layer of the Li−S cell with the CNF/LPS/CNT cathode (Figure 4d and e, areas demarcated in red). In contrast, the lithium sulfide particles with much smaller particle sizes (<250 nm) can be found on the surface of the CNT/Mo layer of the Li−S cell with the CNF/LPS/Mo/CNT cathode (Figure 4f, marked by red arrows). These results highlight the important role of metallic Mo nanoclusters in the uniform deposition of the discharge product. The CNT/Mo cap layer is critical for promoting efficient electron and ion transport across the electrode/electrolyte interfaces, in accordance with the EIS analyses, as shown in Figures S13 and S14, which is beneficial for long-term cycling stability.[58,59] Moreover, the CNF layers of CNF/LPS and CNF/LPS/CNT cathodes both present irregular micrometer-sized agglomerations (Figure 4g and h, marked in red), while the CNF layer of the CNF/LPS/Mo/CNT cathode exhibited no obvious change after the first discharge process (Figure 4i). Therefore, the designed CNF/LPS/Mo/CNT cathode affords strong

DOI: 10.1021/acsnano.9b09135
ACS Nano 2020, 14, 1148−1157

polysulfide chemisorption, fast redox reaction kinetics of the sulfur species, and good structural stability, which contribute collectively to the enhanced electrochemical performance.

The rate capabilities of different cathodes were probed at various current densities (Figure 5a). With the increased current density, the CNF/LPS/Mo/CNT cathode delivers discharge capacities of 1278, 1124, 1044, 953, and 694 mAh g^{-1} at 0.2, 0.5, 1, 2, and 5 *C*, respectively. Moreover, after switching the current density back to 2, 1, 0.5, and 0.2 *C* after the measurement at 5 *C*, the discharge capacities of the CNF/LPS/Mo/CNT electrode revert close to their initial values, suggesting good reversibility. In contrast, the CNF/LPS/CNT and CNF/LPS cathodes depict inferior capacity retention with increasing C rate in comparison to the CNF/LPS/Mo/CNT electrode, suggesting the improved stability of the CNF/LPS/Mo/CNT cathode. Figure 5b displays the charge−discharge profiles of the CNF/LPS/Mo/CNT cathode at different current densities, showing the well-defined voltage plateaus with small polarization potential. The comparison of the voltage hysteresis of the CNF/LPS/Mo/CNT cathode with that of the CNF/LPS and CNF/LPS/CNT cathodes was summarized in Figure 5c and Figure S15. The drastic decrease of the polarization potential for the CNF/LPS/Mo/CNT cathode suggests improved redox reaction kinetics benefiting from the enhanced chemical immobilization and catalytic conversion of polysulfide redox enabled by metallic nanoclusters on the CNT film.

The long-term cycling stability of Li−S cells with different cathodes was measured at a current density of 1 *C* (Figure 5d). The CNF/LPS cathode delivered a discharge capacity of 722 mAh g^{-1} for the first cycle and 261 mAh g^{-1} for the 500th cycle with a low Coulombic efficiency of 95%. The CNF/LPS/CNT cathode showed better capacity retention and higher Columbic efficiency than the CNF/LPS cathode. It demonstrated a discharge capacity of 470 mAh g^{-1} for the 500th cycle with a Coulombic efficiency of 98%. The capacity retention of the CNF/LPS/CNT cathode was 58%, better than 36% for the CNF/LPS cathode (Figure S15). Furthermore, a high reversible discharge capacity of 744 mAh g^{-1} with ∼99.6% Columbic efficiency was achieved for the CNF/LPS/Mo/CNT cathode after 500 cycles at 1 *C* with an average capacity decay of 0.06% per cycle. These data outperform most of the recently reported advanced semiliquid sulfur-based cathodes (see Table S1 for details). In the high-resolution Mo 3d XPS spectra, the electrodes before and after cycling show peaks at the same locations. The peaks at 229.0 and 231.9 eV are assigned to the Mo−Mo bond for metallic Mo (Mo^0), while the peaks at 232.8 and 235.9 eV suggest the presence of MoO_x species.[40,41] Moreover, the Raman spectra and XRD patterns of the CNT/Mo film show the same peaks before and after cycling. These results indicate that the initial metallic Mo particles are stable during long-term cycling. Notably, the Li metal foil from the CNF/LPS/Mo/CNT-based Li−S cell after cycling shows a roughly more compact surface than those from CNF/LPS/CNT- and CNF/LPS-based Li−S cells (Figure S18), further demonstrating the superiority of metallic Mo nanocrystal in relieving the LPS shuttle effect in Li−S batteries, which accounts for the great cycling performance.

The electrochemical performance of a CNF/LPS/Mo/CNT cathode with a high sulfur mass loading was further investigated in consideration of the practical applications (Figure 5e). With a sulfur mass loading of 7.64 mg cm^{-2} (40 μL of 0.5 M Li_2S_6 catholyte), the corresponding specific capacity could reach up to 782.7 mAh g^{-1} (corresponding to an areal capacity of 5.98 mAh cm^{-2}) at the first cycle and sustain a capacity of 621.4 mAh g^{-1} (corresponding to an areal capacity of 4.75 mAh cm^{-2}) after 100 cycles at 0.2 *C* (Figure 5e). The capacity based on the entire weight of all of the components of electrodes including CNF, LPS, and CNT/Mo is still as high as 548.5 mAh g^{-1} after 100 cycles at 0.2 *C*, which is comparable to commercial Li-ion batteries, highlighting the effectiveness of a well-designed CNF/LPS/Mo/CNT cathode. It demonstrated a high capacity retention stabilized at ∼80%, which is considerably higher than many recently reported advanced sulfur-based cathodes with a sulfur mass loading higher than 6 mg cm^{-2} (Table S2). The gravimetric energy densities of the CNF/LPS/Mo/CNT cathode-based Li−S cell are 138.8 W h kg^{-1} based on the mass of active LPS and solvent (see details in Table S3), which is superior to the recently reported advanced sulfur cathode (Table S4). From the above discussion, the metallic Mo clusters on the CNT film significantly improved the electrochemical performance of the sulfur-based cathode. We further compared the electrochemical performance of CNF/LPS/Mo/CNT cathodes with different mass loadings of metallic Mo. As shown in Figure S20, the electrode with a Mo mass loading of 0.05 mg cm^{-2} shows a higher overall capacity than those with Mo mass loadings of 0.01 and 0.1 mg cm^{-2} during the measured cycles. Importantly, the metallic Mo nanocrystals only constitute the 5% weight of the CNF/LPS/Mo/CNT cathode, which still enables excellent electrochemical performance that is comparable with that reported in sulfur-based cathodes with a much higher content of metal compounds (15−50 wt %), definitely highlighting the preponderance of our CNF/LPS/Mo/CNT cathode.

CONCLUSION

In summary, we have successfully fabricated a semiliquid cathode composed of an LPS solution/CNF composite layer and a CNT cap layer decorated with metallic Mo nanoclusters for high-performance Li−S batteries. The conductive CNF network accommodates the LPS catholyte, and the compact CNF/Mo cap layer works as a physical barrier to suppress the shuttle effect of LPS. In spite of their low weight loading, the metallic Mo nanoclusters decorated on the CNT films provide chemical binding sites for LPS, enable faster redox kinetics, and regulate the deposition behaviors of the discharge product. Therefore, the Li−S cell with the CNF/LPS/CNT/Mo cathode delivered a high utilization of active sulfur species (1401 mAh g^{-1} at 0.1 *C*), stable long-term cycling stability (a low decay rate of 0.06% per cycle for 500 cycles at 1 *C*), outstanding rate capability (694 mAh g^{-1} at 5 *C*), and low self-discharge rate. In addition, a high reversible areal capacity of 4.75 mAh cm^{-2} was achieved after 100 cycles at 0.2 *C* for a CNF/LPS/CNT/Mo electrode with a high sulfur loading of 7.64 mg cm^{-2}. Our work sheds light on an alternative strategy toward rational design and structural engineering of electrode materials for high-energy batteries beyond Li-ion technologies.

EXPERIMENTAL SECTION

Preparation of Carbon Nanofiber (CNF) Paper. The free-standing porous CNF paper was prepared *via* a vacuum filtration and CO_2 activation process. Typically, 200 mg of commercial CNF (Showa Denko, a diameter of 150 nm and a length to diameter ratio of 16−18) was dispersed in a mixture (100 mL) of deionized water and isopropyl alcohol (4:1, vol) by ultrasonication for 30 min. Then, a certain volume of the obtained CNF suspension was vacuum-filtered through nylon film (0.45 mm) to form a CNF paper. After dryin at 50 °C, the CNF paper was further cut into small disks with diameters of 8 mm and treated under a flowing CO_2 atmosphere for 2 h at 875 °C with a heating rate of 10 °C min^{-1}.

Preparation of Carbon Nanotube (CNT) Film. The CNT film was prepared *via* a vacuum filtration process. Typically, 100 mg of commercial CNT (Showa Denko, a diameter of 15 nm and a length to diameter ratio of 100−1000) was dispersed into 100 mL of ethanol solution by ultrasonication. To achieve the CNT film, 5 mL of the as-prepared dispersion was vacuum-filtered on the PP separator and vacuum-dried at 60 °C.

Preparation of Metallic Mo Decorated CNT Cap Layer. The decoration of metallic Mo nanoclusters on the CNT film was carried out at room temperature *via* a magnetron sputtering system (JCP500, Beijing Technol Science Co., Ltd.). A cylindrical Mo target with 99.99% purity and a size of 3 in. was used. The working atmosphere was Ar with 99.99% purity, and the pressure was set at 0.45 Pa after reaching the base pressure below 8×10^{-4} Pa. DC power was used and was set at 30 W for low speed to obtain a more uniform coating. The sputtering time was set at 7.5 min with a speed of ∼6 nm/min. The thickness and mass loading of metallic Mo are ∼50 nm and 0.05 mg cm^{-2}, respectively.

Preparation of Electrolyte and LPS Catholyte. The blank electrolyte was prepared by dissolving 10 mmol of lithium bis(trifluoromethanesulfonyl)imide (LiTFSI, Sigma-Aldrich) and 2 mmol of lithium nitrate ($LiNO_3$, Sigma-Aldrich) in 10 mL of dioxolane (DOL, Sigma-Aldrich) and 1,2-dimethoxyethane (DME, Sigma-Aldrich) (1:1, vol). The polysulfide catholyte (0.5 M Li_2S_6) was prepared by chemically reacting sublimed sulfur (S, Aladdin) and lithium sulfide (Li_2S, Sigma-Aldrich) in the blank electrolyte under stirring at 50 °C in an Ar-filled glovebox overnight.

Materials Characterization. The surface chemical composition of CNT/Mo composites was characterized by X-ray photoelectron spectroscopy (XPS, AXIS-ULTRA DLD-600W) and Raman spectroscopy (Horiba JobinYvon, LabRAM HR800). The crystal structure was performed by XRD on a PANalytical B.V. Empyrean operating at 40 kV voltage and 40 mA current with Cu Kα radiation ($\lambda = 0.15406$ nm). Field emission scanning electron microscopy (FESEM, GeminiSEM300) and transmission electron microscopy (TEM, Talos F200X) were performed to identify the surface morphology and structure. To observe the surface morphology and structure of the cycled electrodes, the samples were first extracted from the coin cells in the Ar-filled glovebox followed by a gentle rinse with DOL to remove Li salt residues, and then, they were hermetically sealed inside an aluminum plastic bag before being quickly transferred into the instrument to minimize the exposure to ambient conditions.

Electrochemical Measurements. Standard CR2032 coin-type cells were assembled in an argon-filled glovebox with moisture and oxygen contents below 0.1 ppm. Li metal was used as the anode. 1 M LiTFSI with 2% $LiNO_3$ in DOL/DME (1:1, vol) was used as the electrolyte. A 10 μL portion of Li_2S_6 catholyte (0.5 M), corresponding to a sulfur loading of 1.91 mg cm^{-2}, was added into the porous CNF substrates to form a CNF/LPS composite as the basis for the design of various cathodes. A regular polypropylene (PP) separator, CNT film supported PP separator, and CNT/Mo film supported PP separator were used for the Li||CNF/LPS, Li||CNF/LPS/CNT, and Li||CNF/LPS/Mo/CNT cells, respectively. A 40 μL portion of Li_2S_6 catholyte (0.5 M) was used for the high sulfur loading cathode. Apart from the catholyte, an extra 20 μL of blank electrolyte was used for each cell. The galvanostatic charge/discharge tests were conducted from 1.7 to 2.8 V (vs Li/Li^+) using a LAND 8-channel battery tester. The cyclic voltammetry (CV) and electrochemical impedance spectroscopy (EIS) measurements were performed on a Biologic VMP3 electrochemical workstation. Cyclic voltammetry (CV) curves were collected at a scan rate of 0.1 mV s^{-1}. Electrochemical impedance spectroscopy (EIS) analysis was measured in the frequency range from 100 kHz to 0.01 Hz with 5 mV amplitude.

Symmetric Electrochemical Cell Assembly and Measurements. Symmetric electrochemical cells were assembled by two identical polysulfide hosts (including CNF, CNF/CNT, and CNF/Mo/CNT) with 20 μL of Li_2S_6 catholyte (0.5 M). The CV measurement was performed with a voltage window between −0.7 and 0.7 V under a scan rate of 5 mV s^{-1}. The EIS measurement was conducted at open-circuit voltage in the frequency ranges of 100 kHz to 0.1 Hz with a sinusoidal voltage of an amplitude of 5 mV.

Li_2S Nucleation Tests. Li-catalyst electrochemical cells were assembled by the polysulfide hosts (including CNF, CNF/CNT, and CNF/Mo/CNT) and Li metal anodes with 20 μL of Li_2S_6 catholyte (0.5 M). For Li_2S nucleation tests, the cells were galvanostatically discharged at 50 mA g^{-1} from the open circuit condition to 2.0 V.

ASSOCIATED CONTENT

Supporting Information

The Supporting Information is available free of charge at https://pubs.acs.org/doi/10.1021/acsnano.9b09135.

> Figures S1−S21: additional SEM images, XRD, and Raman data of samples and additional voltage profiles and CVs of prepared cathodes; Table S1−S4: comparison of electrochemical performance and gravimetric energy density of prepared cathodes with other recent reported sulfur-based cathodes (PDF)

AUTHOR INFORMATION

Corresponding Author

*E-mail: yongmingsun@hust.edu.cn.

ORCID

Lin Fu: 0000-0001-6834-2881
Jiang Tang: 0000-0003-2574-2943
Zhi Wei Seh: 0000-0003-0953-567X
Yongming Sun: 0000-0001-8528-525X

Notes

The authors declare no competing financial interest.

ACKNOWLEDGMENTS

Y.S. acknowledges the financial support by the Innovation Fund of Wuhan National Laboratory for Optoelectronics of Huazhong University of Science and Technology. The authors would like to thank the Analytical and Testing Center of Huazhong University of Science and Technology as well as the Center for Nanoscale Characterization & Devices of Wuhan National Laboratory for Optoelectronics for providing the facilities to conduct the characterization. E.M. acknowledges the support of the Fundamental Research Funds for the Central Universities, Huazhong University of Science and Technology (2019JYCXJJ014). Z.W.S. acknowledges the support of the Singapore National Research Foundation (NRF-NRFF2017-04).

REFERENCES

(1) Bruce, P. G.; Freunberger, S. A.; Hardwick, L. J.; Tarascon, J.-M. Li-O_2 and Li-S Batteries with High Energy Storage. *Nat. Mater.* **2012**, *11*, 19−29.

(2) Seh, Z. W.; Sun, Y.; Zhang, Q.; Cui, Y. Designing High-Energy Lithium-Sulfur Batteries. *Chem. Soc. Rev.* **2016**, *45*, 5605−5634.

(3) Manthiram, A.; Fu, Y.; Chung, S.-H.; Zu, C.; Su, Y.-S. Rechargeable Lithium-Sulfur Batteries. *Chem. Rev.* **2014**, *114*, 11751−11787.

(4) Xue, W. J.; Shi, Z.; Suo, L. M.; Wang, C.; Wang, Z. Q.; Wang, H. Z.; So, K. P.; Manurano, A.; Yu, D. W.; Chen, Y. M.; Qie, L.; Zhu, Z.; Xu, G.; Kong, J.; Li, J. Intercalation-Conversion Hybrid Cathodes Enaling Li-S Full-Cell Architectures with Jointly Superior Gravimetric and Volumetric Energy Densities. *Nat. Energy* **2019**, *4*, 374−382.

(5) Cao, Y. L.; Li, M.; Lu, J.; Liu, J.; Amine, K. Bridging the Academic and Industrial Metrics for Next-Generation Practical Batteries. *Nat. Nanotechnol.* **2019**, *14*, 200−207.

(6) Tu, S.; Chen, X.; Zhao, X.; Cheng, M.; Xiong, P.; He, Y.; Zhang, Q.; Xu, Y. A Polysulfide-Immobilizing Polymer Retards the Shuttling of Polysulfide Intermediates in Lithium-Sulfur Batteries. *Adv. Mater.* **2018**, *30*, 1804581.

(7) Li, Y.; Wang, W.; Liu, X.; Mao, E.; Wan, M.; Li, G.; Fu, L.; Li, Z.; Eng, A. Y. S.; Seh, Z. W.; Sun, Y. Engineering Stable Electrode-Separator Interfaces with Ultrathin Conductive Polymer Layer for High-Energy-Density Li-S Batteries. *Energy Storage Mater.* **2019**, *23*, 261−268.

(8) Pang, Q.; Shyamsunder, A.; Narayanan, B.; Kwok, C. Y.; Curtiss, L. A.; Nazar, L. F. Tuning the Electrolyte Network Structure to Invoke Quasi-Solid State Sulfur Conversion and Suppress Lithium Dendrite Formation in Li-S Batteries. *Nat. Energy* **2018**, *3*, 783−791.

(9) Li, Z.; Zhang, J.; Guan, B.; Wang, D.; Liu, L.-M.; Lou, X. W. A Sulfur Host Based on Titanium Monoxide@Carbon Hollow Spheres for Advanced Lithium-Sulfur Batteries. *Nat. Commun.* **2016**, *7*, 13065.

(10) Ji, X.; Lee, K. T.; Nazar, L. F. A Highly Ordered Nanostructured Carbon-Sulphur Cathode for Lithium-Sulphur Batteries. *Nat. Mater.* **2009**, *8*, 500−506.

(11) Li, M.; Carter, R.; Douglas, A.; Oakes, L.; Pint, C. L. Sulfur Vapor-Infiltrated 3D Carbon Nanotube Foam for Binder-Free High Areal Capacity Lithium-Sulfur Battery Composite Cathodes. *ACS Nano* **2017**, *11*, 4877−4884.

(12) Pei, F.; Lin, L.; Ou, D.; Zheng, Z.; Mo, S.; Fang, X.; Zheng, N. Self-Supporting Sulfur Cathodes Enabled by Two-Dimensional Carbon Yolk-Shell Nanosheets for High-Energy-Density Lithium Sulfur Batteries. *Nat. Commun.* **2017**, *8*, 482.

(13) Fu, Y.; Su, Y.-S.; Manthiram, A. Highly Reversible Lithium/Dissolved Polysulfide Batteries with Carbon Nanotube Electrodes. *Angew. Chem., Int. Ed.* **2013**, *52*, 6930−6935.

(14) Qie, L.; Zu, C.; Manthiram, A. A High Energy Lithium-Sulfur Battery with Ultrahigh-Loading Lithium Polysulfide Cathode and Its Failure Mechanism. *Adv. Energy Mater.* **2016**, *6*, 1502459.

(15) Zhou, G.; Paek, E.; Hwang, G. S.; Manthiram, A. Long-life Li/Polysulphide Batteries with High Sulphur Loading Enabled by Lightweight Three-Dimensional Nitrogen/Sulphur-Codoped Graphene Sponge. *Nat. Commun.* **2015**, *6*, 7760.

(16) Pu, X.; Yang, G.; Yu, C. Liquid-Type Cathode Enabled by 3D Sponge-Like Carbon Nanotubes for High Energy Density and Long Cycling Life of Li-S Batteries. *Adv. Mater.* **2014**, *26*, 7456−7461.

(17) Li, X.; Pu, X.; Han, S.; Liu, M.; Du, C.; Jiang, C.; Huang, X.; Liu, T.; Hu, W. Enhanced Performances of Li/Polysulfide Batteries with 3D Reduced Graphene Oxide/Carbon Nanotube Hybrid Aerogel as the Polysulfide Host. *Nano Energy* **2016**, *30*, 193−199.

(18) Liang, X.; Hart, C.; Pang, Q.; Garsuch, A.; Weiss, T.; Nazar, L. F. A Highly Efficient Polysulfide Mediator for Lithium-Sulfur Batteries. *Nat. Commun.* **2015**, *6*, 5682.

(19) Pan, Z.-Z.; Lv, W.; He, Y.-B.; Zhao, Y.; Zhou, G.; Dong, L.; Niu, S.; Zhang, C.; Lyu, R.; Wang, C.; Shi, H.; Zhang, W.; Kang, F.; Nishihara, H.; Yang, Q.-H. A Nacre-Like Carbon Nanotube Sheet for High Performance Li-Polysulfde Batteries with High Sulfur Loading. *Adv. Sci.* **2018**, *5*, 1800384.

(20) Wang, X.; Gao, T.; Han, F.; Ma, Z.; Zhang, Z.; Li, J.; Wang, C. Stabilizing High Sulfur Loading Li-S Batteries by Chemisorption of Polysulfide on Three-Dimensional Current Collector. *Nano Energy* **2016**, *30*, 700−708.

(21) Chung, S.-H.; Luo, L.; Manthiram, A. TiS_2-Polysulfide Hybrid Cathode with High Sulfur Loading and Low Electrolyte Consumption for Lithium-Sulfur Batteries. *ACS Energy Lett.* **2018**, *3*, 568−573.

(22) Zhou, G.; Zhao, Y.; Zu, C.; Manthiram, A. Free-standing TiO_2 Nanowire-Embedded Graphene Hybrid Membrane for Advanced Li/Dissolved Polysulfide Batteries. *Nano Energy* **2015**, *12*, 240−249.

(23) Li, Z.; He, Q.; Xu, X.; Zhao, Y.; Liu, X.; Zhou, C.; Ai, D.; Xia, L.; Mai, L. A 3D Nitrogen-Doped Graphene/TiN Nanowires Composite as a Strong Polysulfide Anchor for Lithium-Sulfur Batteries with Enhanced Rate Performance and High Areal Capacity. *Adv. Mater.* **2018**, *30*, 1804089.

(24) Luo, L.; Chung, S.-H.; Manthiram, A. A Three-Dimensional Self-Assembled SnS_2-Nano-Dots@Graphene Hybrid Aerogel as an Efficient Polysulfide Reservoir for High-Performance Lithium−Sulfur Batteries. *J. Mater. Chem. A* **2018**, *6*, 7659−7667.

(25) Li, L.; Chen, L.; Mukherjee, S.; Gao, J.; Sun, H.; Liu, Z.; Ma, X.; Gupta, T.; Singh, C. V.; Ren, W.; Cheng, H.-M.; Koratkar, N. Phosphorene as a Polysulfide Immobilizer and Catalyst in High-Performance Lithium-Sulfur Batteries. *Adv. Mater.* **2017**, *29*, 1602734.

(26) Song, J.; Guo, X.; Zhang, J.; Chen, Y.; Zhang, C.; Luo, L.; Wang, F.; Wang, G. Rational Design of Free-standing 3D Porous MXene/rGO Hybrid Aerogels as Polysulfide Reservoirs for High-Energy Lithium-Sulfur Batteries. *J. Mater. Chem. A* **2019**, *7*, 6507.

(27) Zhou, F.; Li, Z.; Luo, X.; Wu, T.; Jiang, B.; Lu, L.-L.; Yao, H.-B.; Antonietti, M.; Yu, S.-H. Low Cost Metal Carbide Nanocrystals as Binding and Electrocatalytic Sites for High Performance Li-S Batteries. *Nano Lett.* **2018**, *18*, 1035−1043.

(28) Sun, Z.; Zhang, J.; Yin, L.; Hu, G.; Fang, R.; Cheng, H.-M.; Li, F. Conductive Porous Vanadium Nitride/Graphene Composite as Chemical Anchor of Polysulfides for Lithium-Sulfur Batteroes. *Nat. Commun.* **2017**, *8*, 14627.

(29) Zha, C.; Wu, D.; Zhang, T.; Wu, J.; Chen, H. A Facile and Effective Sulfur Loading Method: Direct Drop of Liquid Li_2S_8 on Carbon Coated TiO_2 Nanowire Arrays as Cathode towards Commercializing Lithium-Sulfur Battery. *Energy Storage Mater.* **2019**, *17*, 118−125.

(30) Chung, S.-H.; Manthiram, A. Designing Lithium-Sulfur Cells with Practically Necessary Parameters. *Joule* **2018**, *2*, 710−724.

(31) Al Salem, H.; Babu, G.; V. Rao, C.; Arava, L. M. R. Electrocatalytic Polysulfide Traps for Controlling Redox Shuttle Process of Li-S Batteries. *J. Am. Chem. Soc.* **2015**, *137*, 11542−11545.

(32) Zhang, L.; Chen, X.; Wang, F.; Niu, Z.; Wang, Y.; Zhang, Q.; Chen, J. Enhanced Electrochemical Kinetics and Polysulfide Traps of Indium Nitride for Highly Stable Lithium-Sulfur Batteries. *ACS Nano* **2018**, *12*, 9578−9586.

(33) Lin, H.; Yang, L.; Jiang, X.; Li, G.; Zhang, T.; Yao, Q.; Zheng, G. W.; Lee, J. Y. Electrocatalysis of Polysulfide Conversion by Sulfur-Deficient MoS_2 Nanoflakes for Lithium-Sulfur Batteries. *Energy Environ. Sci.* **2017**, *10*, 1476.

(34) Liu, X.-C.; Zhou, S. P.; Liu, M.; Xu, G.-L.; Zhou, X.-D.; Huang, L.; Sun, S.-G.; Amine, K.; Ke, F.-S. Utilizing a Metal as a Sulfur Host for High Performance Li-S Batteries. *Nano Energy* **2018**, *50*, 685−690.

(35) Fang, D.; Wang, Y.; Qian, C.; Liu, X.; Wang, X.; Chen, S.; Zhang, S. Synergistic Regulation of Polysulfides Conversion and Deposition by MOF-Derived Hierarchically Ordered Carbonaceous Composite for High-Energy Lithium-Sulfur Batteries. *Adv. Funct. Mater.* **2019**, *29*, 1900875.

(36) Yao, H.; Zheng, G.; Hsu, P. C.; Kong, D.; Cha, J. J.; Li, W.; Seh, Z. W.; McDowell, M. T.; Yan, K.; Liang, Z.; Narasimhan, V. K.; Cui, Y. Improving Lithium-Sulphur Batteries Through Spatial Control of Sulphur Species Deposition on a Hybrid Electrode Surface. *Nat. Commun.* **2014**, *5*, 3943.

(37) Yuan, H.; Peng, H.-J.; Li, B.-Q.; Xie, J.; Kong, L.; Zhao, M.; Chen, X.; Huang, J.-Q.; Zhang, Q. Conductive and Catalytic Triple-Phase Interfaces Enabling Uniform Nucleation in High-Rate Lithium-Sulfur Batteries. *Adv. Energy Mater.* **2019**, *9*, 1802768.

(38) Pan, H.; Chen, J.; Cao, R.; Murugesan, V.; Rajput, N. N.; Han, K. S.; Persson, K.; Estevez, L.; Engelhard, M. H.; Zhang, J.-G.; Mueller, K. T.; Cui, Y.; Shao, Y.; Liu, J. Non-Encapsulation Approach for High-Performance Li-S Batteries through Controlled Nucleation and Growth. *Nat. Energy* **2017**, *2*, 813−820.

(39) Qie, L.; Manthiram, A. A Facile Layer-by-Layer Approach for High-Areal-Capacity Sulfur Cathodes. *Adv. Mater.* **2015**, *27*, 1694−1700.

(40) Yue, X.-Y.; Li, X.-L.; Meng, J.-K.; Wu, X.-J.; Zhou, Y.-N. Padding Molybdenum Net with Graphite/MoO_3 Composite as a Multifunctional Interlayer Enabling High-Performance Lithium-Sulfur Batteries. *J. Power Sources* **2018**, *397*, 150−156.

(41) Yang, W.; Xiao, J.; Ma, Y.; Cui, S.; Zhang, P.; Zhai, P.; Meng, L.; Wang, X.; Wei, Y.; Du, Z.; Li, B.; Sun, Z.; Yang, S.; Zhang, Q.; Gong, Y. Tin Intercalated Ultrathin MoO_3 Nanoribbons for Advanced Lithium-Sulfur Batteries. *Adv, Energy. Mater.* **2019**, *9*, 1803137.

(42) Fang, R.; Zhao, S.; Sun, Z.; Wang, D.-W.; Amal, R.; Wang, S.; Cheng, H.-M.; Li, F. Polysulfide Immobilization and Conversion on a Conductive Polar MoC@MoO_x Material for Lithium-Sulfur Batteries. *Energy Storage Mater.* **2018**, *10*, 56−61.

(43) Wang, C.; Li, K.; Zhang, F.; Wu, Z.; Sun, L.; Wang, L. Insight of Enhanced Redox Chemistry for Porous MoO_2 Carbon Derived Framework as Polysulfide Reservoir in Lithium-Sulfur Batteries. *ACS Appl. Mater. Interfaces* **2018**, *10*, 42286−42293.

(44) Imtiaz, S.; Zafar, Z. A.; Razaq, R.; Sun, D.; Xin, Y.; Li, Q.; Zhang, Z.; Zheng, L.; Huang, Y.; Anderson, J. A. Electrocatalysis on Separator Modifed by Molybdenum Trioxide Nanobelts for Lithium-Sulfur Batteries. *Adv. Mater. Interfaces* **2018**, *5*, 1800243.

(45) Wu, X.; Du, Y.; Wang, P.; Fan, L.; Cheng, J.; Wang, M.; Qiu, Y.; Guan, B.; Wu, H.; Zhang, N.; Sun, K. Kinetics Enhancement of Lithium-Sulfur Batteries by Interlinked Hollow MoO_2 Sphere/Nitrogen-Doped Graphene Composite. *J. Mater. Chem. A* **2017**, *5*, 25187−25192.

(46) Zhang, Q.; Wang, Y.; She, Z. W.; Fu, Z.; Zhang, R.; Cui, Y. Understanding the Anchoring Effect of Two-Dimensional Layered Materials for Lithium-Sulfur Batteries. *Nano Lett.* **2015**, *15*, 3780−3786.

(47) Yao, H.; Yan, K.; Li, W.; Zheng, G.; Kong, D.; Seh, Z. W.; Narasimhan, V. K.; Liang, Z.; Cui, Y. Improved Lithium−Sulfur Batteries with a Conductive Coating on the Separator to Prevent the Accumulation of Inactive S-Related Species at the Cathode-Separator Interface. *Energy Environ. Sci.* **2014**, *7*, 3381−3390.

(48) Huang, J.-Q.; Zhang, Q.; Peng, H.-J.; Liu, X.-Y.; Qian, W.-Z.; Wei, F. Ionic Shield for Polysulfides towards Highly-Stable Lithium-Sulfur Batteries. *Energy Environ. Sci.* **2014**, *7*, 347−353.

(49) Wang, L.; Liu, J.; Yuan, L.; Wang, Y.; Xia, Y. To Mitigate Self-Discharge of Lithium-Sulfur Batteries by Optimizing Ionic Liquid Electrolytes. *Energy Environ. Sci.* **2016**, *9*, 224.

(50) Ma, L.; Lin, H.; Zhang, W.; Zhao, P.; Zhu, G.; Hu, Y.; Chen, R.; Tie, Z.; Liu, J.; Jin, Z. Nitrogen-Doped Carbon Nanotube Forests Planted on Cobalt Nanoflowers as Polysulfide Mediator for Ultralow Self-Discharge and High Areal-Capacity Lithium-Sulfur Batteries. *Nano Lett.* **2018**, *18*, 7949−7954.

(51) Du, Z.; Chen, X.; Hu, W.; Chuang, C.; Xie, S.; Hu, A.; Yan, W.; Kong, X.; Wu, X.; Ji, H.; Wan, L.-J. Cobalt in Nitrogen-Doped Graphene as Single-Atom Catalyst for High-Sulfur Content Lithium-Sulfur Batteries. *J. Am. Chem. Soc.* **2019**, *141*, 3977−3985.

(52) Lin, H.; Zhang, S.; Zhang, T.; Cao, S.; Ye, H.; Yao, Q.; Zheng, G.; Lee, J. Y. A Cathode-Integrated Sulfur-Deficient Co_9S_8 Catalytic Interlayer for the Reutilization of "Lost" Polysulfides in Lithium-Sulfur Batteries. *ACS Nano* **2019**, *13*, 7073−7082.

(53) Lin, H.; Zhang, S.; Zhang, T.; H, Y.; Y, Q.; Zheng, G.; Lee, J. Y. Simultaneous Cobalt and Phosphorous Doping of MoS_2 for Improved Catalytic Performance on Polysulfide Conversion in Lithium-Sulfur Batteries. *Adv. Energy Mater.* **2019**, *9*, 1902096.

(54) Eng, A. Y. S.; Liang, E. J.; Lee, S. S. Controlled Synthesis of Transition Metal Disulfides (MoS_2 and WS_2) on Carbon Fibers: Effects of Phase and Morphology toward Lithium-Sulfur Battery Performance. *Appl. Mater. Today* **2019**, *16*, 529−537.

(55) He, J.; Hartmann, G.; Lee, M.; Hwang, G. S.; Chen, Y.; Manthiram, A. Freestanding 1T MoS_2/Graphene Heterostructures as a Highly Efficient Electrocatalyst for Lithium Polysulfides in Li-S Batteries. *Energy Environ. Sci.* **2019**, *12*, 344−350.

(56) Pang, Q.; Kwok, C. Y.; Kundu, D.; Liang, X.; Nazar, L. F. Lightweight Metallic MgB_2 Mediates Polysulfide Redox and Promises High-Energy Density Lithium-Sulfur Batteries. *Joule* **2019**, *3*, 136−148.

(57) Yu, M.; Zhou, S.; Wang, Z.; Wang, Y.; Zhang, N.; Wang, S.; Zhao, J.; Qiu, J. Accelerating Polysulfide Redox Conversion on Bifunctional Electrocatalytic Electrode for Stable Li-S Batteries. *Energy Storage Mater.* **2019**, *20*, 98−107.

(58) Tsao, Y.; Lee, M.; Miller, E. C.; Gao, G.; Park, J.; Chen, S.; Katsumata, T.; Tran, H.; Wang, L.-W.; Toney, M. F.; Cui, Y.; Bao, Z. Designing a Quinone-Based Redox Mediator to Facilitate Li_2S Oxidation in Li-S Batteries. *Joule* **2019**, *3*, 872−884.

(59) Peng, H.-J.; Huang, J.-Q.; Liu, X.-Y.; Cheng, X.-B.; Xu, W.-T.; Zhao, C.-Z.; Wei, F.; Zhang, Q. Healing High-Loading Sulfur Electrodes with Unprecedented Long Cycling Life: Spatial Heterogeneity Control. *J. Am. Chem. Soc.* **2017**, *139*, 8458−8466.